Article

Adsorption of Malachite Green Dye onto Mesoporous Natural Inorganic Clays: Their Equilibrium Isotherm and Kinetics Studies

Sami Ullah [1], Altaf Ur Rahman [2], Fida Ullah [3], Abdur Rashid [4], Tausif Arshad [1], Eva Viglašová [5], Michal Galamboš [5], Niyaz Mohammad Mahmoodi [6] and Haseeb Ullah [7,*]

[1] Department of Civil Engineering, Mirpur University of Science and Technology, Mirpur 10250, Pakistan; eng.sami07@gmail.com (S.U.); tausif.ce@must.edu.pk (T.A.)

[2] Department of Physics, Riphah International University, Lahore 54000, Pakistan; altaf.urrahman@riphah.edu.pk

[3] Department of Chemistry, Hazara University, Mansehra 21300, Pakistan; fida95229@gmail.com

[4] Department of Environmental Sciences, Quaid-i-Azam University, Islamabad 45320, Pakistan; abdur.rashid@bs.qau.edu.pk

[5] Department of Nuclear Chemistry, Faculty of Natural Sciences, Comenius University in Bratislava, Mlynská Dolina, Ilkovičova 6, 842 15 Bratislava, Slovakia; eva.viglasova@uniba.sk (E.V.); michal.galambos@uniba.sk (M.G.)

[6] Department of Environmental Research, Institute for Color Science and Technology, Tehran 15119, Iran; mahmoodi@icrc.ac.ir

[7] Department of Chemistry, Quaid-i-Azam University, Islamabad 45320, Pakistan

* Correspondence: chemist.ktk.06@gmail.com

Abstract: Contamination of water with organic dyes is a major environmental concern as it causes serious life-threatening environmental problems. The present research was designed to evaluate the potential of three different natural inorganic clays (NICs) i.e., Pakistani bentonite clay (PB), bentonite purchased from Alfa Aesar (BT), and Turkish red mud (RM) for malachite green (MG) dye removal from an aqueous solution. Various analytical techniques, namely X-ray fluorescence spectrometry (XRF), X-ray diffractometry (XRD), Fourier transform infrared spectroscopy (FTIR), field emission scanning electron microscopy (FESEM), Brunauer–Emmett–Teller surface area measurement (BET), and thermogravimetric analysis (TGA), were used to investigate the physicochemical properties of the NICs samples. The effect of adsorption operational parameters such as contact time, aqueous phase pH, dye concentration, and amount of NICs on the adsorption behavior of MG onto NICs samples were investigated under the batch adsorption system. The equilibrium and kinetic inspection reflected the best description of MG adsorption behavior by the Langmuir isotherm model and pseudo-first-order kinetic model, respectively. The results indicated that the adsorption was favorable at higher pH. The maximum adsorption capacities calculated by Langmuir isotherm for PB, BT, and RM were found to be 243.90 mg/g, 188.68 mg/g, and 172.41 mg/g, respectively. It can be concluded that natural inorganic clays with a higher surface area can be used as an effective adsorbent material to remove the MG dye from an aqueous solution.

Keywords: clay; dye; adsorption; isotherm; kinetics

1. Introduction

In recent years, planners, environmental scientists, and decision-makers have been paying attention to sustainable resource development [1]. Within these resources, water is the most precious renewable natural resource, is the essential enabler, and a major source of survival of life [2,3]. Groundwater is the most important source of drinking water in the world [4]. Globally, groundwater accounts for about 43% of total irrigation use and provides potable water for about 1.5 billion people [5]. However, the rapid development of industrialization, manifold increase in the human population growth, and uncontrolled usage of

freshwater have imposed stress on groundwater resources, resulting in quality deterioration and quantity depletion [6,7]. It has been reported that more than 1.2 billion people around the world have no access to potable water, and around 663 million people are being affected by unsafe water [8,9]. Mainly, surface water and groundwater are contaminated due to the discharge of partially treated or untreated wastewater from various industries into the ecosystem. In particular organic dyes from industrial effluents such as textile, solar cells, leather, plastics, food, and paper cause serious health issues in humans and severe damages to the environment [10]. Over 1×10^5 types of dyes and more than 7×10^5 tons per year of pigments and dyestuff are produced and used in many industries, in which 12% is lost during the manufacturing process, and 20% of dyes enter freshwater resources as industrial effluents [11]. Due to their complex structures, organic dyes are mainly non-biodegradable and are resistant to environmental conditions such as heat, oxidizing agents, and light [12,13]. Moreover, most of the dyes are carcinogenic, mutagenic, and harmful to humans and aquatic biota [14]. In addition their high stability towards environmental conditions and resistance to the attack of microorganisms, the presence of organic dyes causes aesthetic problems, impedes penetration of light into receiving water bodies, and depletes dissolved oxygen, thereby disturbing the ecological aquatic systems [15,16].

Malachite green (MG) dye is an organic compound of triphenylmethane, widely used as a colorant [17], biocide in the aquacultural industry [18], therapeutic agent, anthelminthic, and medical disinfectant [19,20]. Despite its wide application, several reports describe its carcinogenic and hazardous effects. It acts as a tumor-promoting agent in mammalian liver cells [21]. Therefore, the detection of MG in foodstuff, fishes, and animal milk used by humans is of great concern [22].

Several techniques have been applied for the decontamination of wastewater containing organic dyes such as adsorption [23], photocatalysis [24], biological treatment [25], chemical oxidation [26], coagulation/flocculation [27], membrane filtration [28], and ozonation [29]. Among different methods, adsorption is a more suitable and prime treatment method, because of the simplicity of design, inexpensiveness, ease of operation, and high efficiency [30]. Initially, activated carbons were the most commonly used adsorbent [31], but the regeneration difficulties and high production cost tend to limit its use as a potential adsorbent [32]. These limitations have encouraged scientists to explore abundant, cheaper, and highly efficient adsorbents such as bio-sorbents, natural materials, and waste materials [33–35].

The utilization of clays and clay minerals as an alternative adsorbent has many advantages, such as environmental friendliness, low cost, higher surface area, abundance and ease in availability, chemical stability, and a high potential for chemical modification [36–38]. Mainly, clays have layered structures and adsorb harmful substances between their layer spaces [39]. Depending on the target pollutants, clays can be used as an adsorbent both in natural and/or modified form [40]. Among the various types of clay, bentonite is the most utilized clay material, mainly composed of at least 50% smectite, and more precisely montmorillonite. Bentonite represents a 2:1 phyllosilicate, consisting of an octahedral alumina sheet sandwiched between two tetrahedral silica sheets [41]. The overall negative charge on the bentonite clay, being caused by the isomorphous substitution of Al^{+3} for Si^{+4} in the tetrahedral layer and Mg^{+2} for Al^{+3} in the octahedral layer, is balanced by the exchangeable cations located in the interlayer spaces, such as Na^+, K^+, and Ca^{+2} [42].

The objective of the current research work was to assess the ability of mesoporous natural inorganic clays (NICs) for the removal of MG dye from an aqueous solution. The influence of adsorption time, aqueous phase pH, MG concentration, and the amount of NICs on the decolorization capabilities of NICs were evaluated. The obtained adsorption results were analyzed by different kinetic and isotherm models.

2. Materials and Methods

2.1. Materials

The NICs adsorbents were obtained: bentonite from Pakistan (PB), bentonite purchased from Alfa Aesar (BT), and red mud from Turkey (RM). The NICs samples were

ground and washed with boiled distilled water followed by a filtration process to remove the soluble impurities. After that, NICs samples were then dried in an oven for 24 h at 80 °C and ground. Sodium hydroxide, hydrochloric acid, and malachite green is a water-soluble cationic dye that belongs to the triphenylmethane category (chemical formula: $C_{23}H_{25}ClN_2$, color index number = 42,000, molar mass: 364.91 g/mol, abbreviated as MG) were obtained from Sigma Aldrich, and used without further pre-treatment. The structure of the MG is shown in Figure 1.
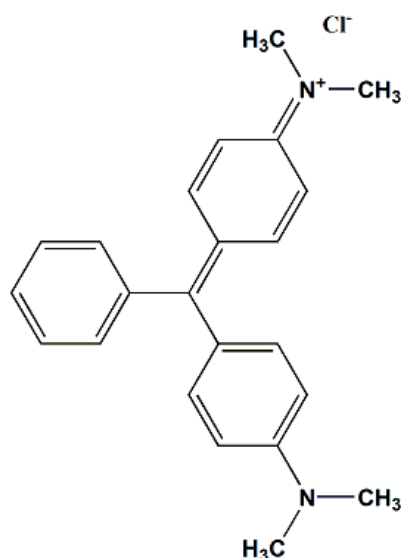
Figure 1. Chemical structure of MG dye.

2.2. Pretreatment of NICs Samples

All of the NICs samples were pretreated as follows: the NICs samples were suspended in distilled water for 4 h and cleaned many times with freshly prepared distilled water. The clean NICs were then oven-dried for 24 h at 105 °C. Finally, the dried NICs materials were stored in sealed jars for further use, without any further physical or chemical treatment.

2.3. Characterization of NICs

To evaluate the mechanism of dye adsorption, it is imperative to examine the characteristics of the adsorbent materials. Therefore, the physicochemical characterizations of the adsorbent materials were analyzed by using various analytical techniques. The chemical composition and elemental analysis of NICs were determined by X-ray fluorescence spectroscopy (XRF) using Bruker Tiger S8 XRF Spectrometer. The X-ray diffraction (XRD) patterns using Bruker D-2 Phaser, Cu Kα radiation over a 2θ interval of 4°–40° were performed to investigate the crystallinity and phase composition of the NICs adsorbents. A Fourier transform infrared spectroscopic (FTIR) analysis was performed by using Bruker-Tensor-27 between 400 to 4000 cm^{-1} for the examination of surface functional groups of NICs. A field emission scanning electron microscopic (FESEM) analysis was performed to determine the NICs adsorbent morphologies using FESEM-EDS (Zeiss Ultra Plus). The Brunauer–Emmett–Teller (BET) nitrogen physisorption measurements were performed using a BET Micromeritics ASAP 2020 instrument for the calculations of pore sizes and specific surface area of the NICs adsorbents. The thermogravimetric analysis (TGA) measurements were carried out using the TGA Q500 model instrument, a nitrogen atmosphere (60 mL/min of N_2), and the samples were heated at 10 °C per minute rise over the temperature range of 25–800 °C.

2.4. Batch Adsorption Studies

To evaluate the adsorption abilities of NICs adsorbents, batch adsorption experiments were performed using 250 mL conical flasks containing 100 mL of working solutions. The influence of operating parameters such as time (10–120 min), NICs amount (0.1–0.5 g), dye concentration (100–350 mg/L), and pH (3–11) on MG dye remediation was investigated in batch studies. Typically, 0.1 g of NICs and MG solution (100 mL) with the desired pH and concentration were added to a 250 mL conical flask and stirred continuously. At pre-determined intervals, the NICs samples were separated. The remaining concentration of MG in the filtrate was spectrophotometrically measured by a UV-vis spectrophotometer (Shimadzu UV1700 Japan).

The adsorbed amount of MG (mg/g) was calculated using the following equations:

$$q_e = \frac{(C_0 - C_e) \times V}{M} \tag{1}$$

where V (L) represents the volume of MG solution, C_o (mg/L) is the initial *MG* concentration, C_e (mg/L) is the concentration at equilibrium, and M (g) is the amount of NICs.

3. Result and Discussion

3.1. Characterization of NICs

The XRF analysis was carried out to investigate the chemical compositions of the NICs used adsorbents. Table 1 shows that PB and BT clays are mainly composed of alumina and silica, while the major components of the RM clay are iron oxide, alumina, and silica, with other oxides present in trace amount in all of the NICs samples. Figure 2 shows the major chemical constituents present in NICs samples.

Table 1. Chemical composition of NICs clay.

Parameter	Chemical Composition (%)		
	PB Clay	**BT Clay**	**RM Clay**
Al_2O_3	56.3	60.7	18.7
SiO_2	18	16.4	15.3
Fe_2O_3	10.5	5.54	44.34
CaO	4.41	4.68	1.36
K_2O	3.51	1.1	0.38
MgO	3.1	3.4	0.47
Na_2O	1.6	6.8	12
TiO_2	1.21	0.63	6.27
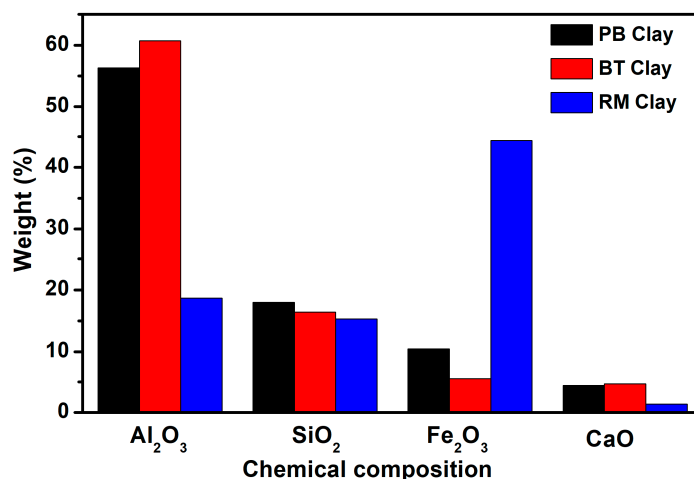
Figure 2. Major chemical constituents of the natural inorganic clays (NICs) adsorbents.

XRD analysis was employed to examine the mineralogical composition and crystalline nature of the NICs samples, as shown in Figure 3. The results indicate that PB and BT clay has the following mineral phases: illite, kaolinite, quartz, and calcite. The dominant diffraction peaks for the PB and BT clays were found at Bragg's angle (2θ) = ~9°, ~12.5°, ~27°, ~28°, and ~29° which corresponds to illite, kaolinite, quartz, feldspars, and calcite, respectively [43,44]. According to the XRD data, RM is mainly composed of hematite, with other minerals such as gibbsite, diaspore, and calcite being present as minor constituents [45].
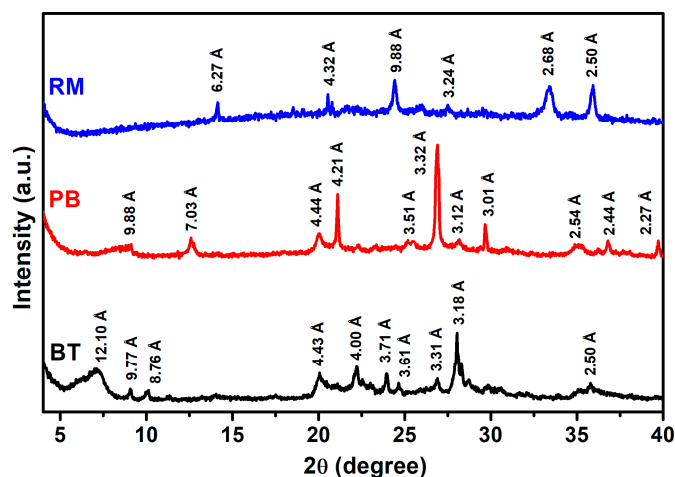
Figure 3. XRD patterns of bentonite purchased from Alfa Aesar (BT), Pakistani bentonite clay (PB), and Turkish red mud (RM) adsorbent.

The surface functional groups of NICs investigated by the accomplishment of FTIR analysis are shown in Figure 4. The results indicated the presence of characteristic absorption bands of NICs at 3696 cm^{-1} belonging to the O-H stretching vibrations of the inner surface hydroxyl group and 3612–3616 cm^{-1} belonging to the O-H stretching vibrations of the structural hydroxyl [46]. The broadbands 3386–3422 cm^{-1} were due to the stretching vibration of H-O-H of hydrogen-bonded inter-layer water molecules [47], while the bands of OH deformation mode of coordinated water molecules appeared at 1632–1641 cm^{-1} [48]. The strong bands at 970–998 cm^{-1} were referred to as the Si-O-Si stretching vibrations [49]. The Si-O bending vibration and Si-O-Mg, Si-O-Si, and Si-O-Al stretching vibrations of the NICs adsorbents were found in the range of 415–796 cm^{-1} [50,51].
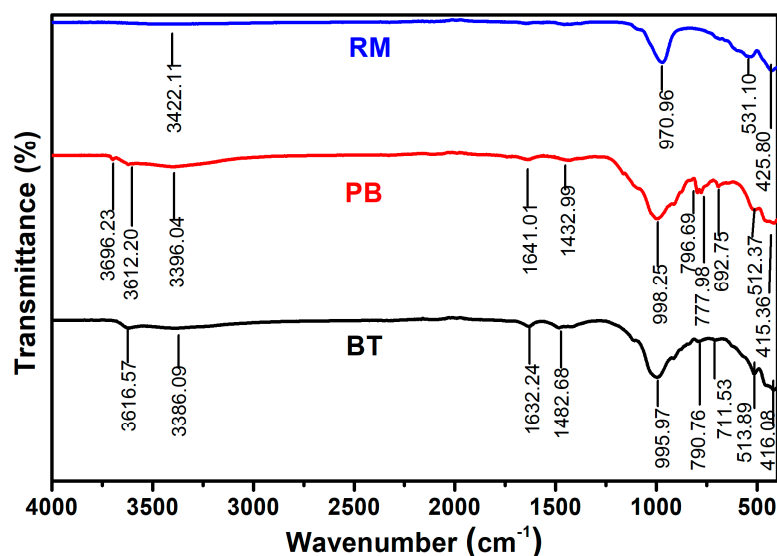
Figure 4. FTIR spectra of RM, PB, and BT adsorbent.

The NICs adsorbent morphologies were analyzed by SEM analysis (Figure 5). It was observed that PB and BT clays have quite a rough porous surface with blunt edges due to the agglomeration of small particle size, while the RM clay has a smooth surface compared to the other two clays and a fluffy appearance because of the closely packed flakes.
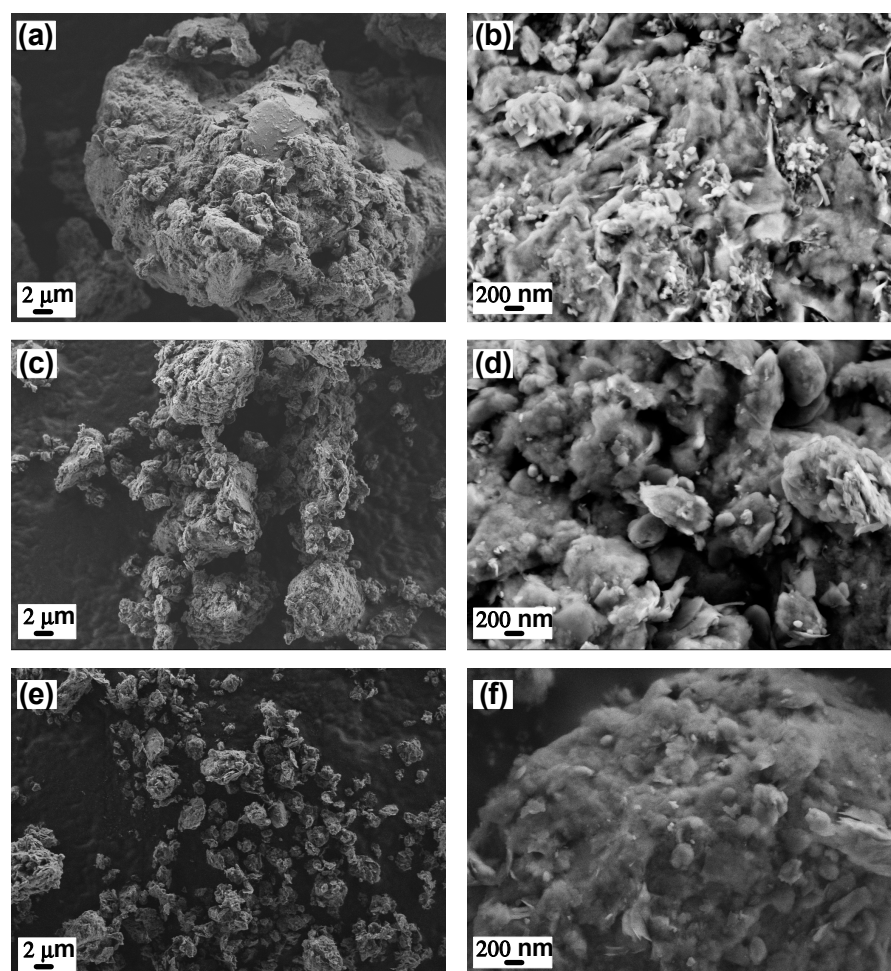

Figure 5. SEM images of (**a**,**b**) BT, (**c**,**d**) PB, and (**e**,**f**) RM adsorbent.

The pore size distribution and surface area of the NICs materials were determined by BET N_2 sorption isotherm analysis. Figure 6 shows that the observed sorption isotherms are of type IV with an H3 type of hysteresis loops. The results confirm the mesoporous nature of the used NICs adsorbents [52]. Both the adsorption-desorption isotherms completely overlapped at low relative pressure $P/P_o < 0.4$, but showed a distinct hysteresis loop at relatively high pressure ($P/P_o > 0.4$), which is the typical characteristics of layered materials. The calculated pore sizes and surface area derived from BET N_2 sorption isotherm of the NICs are given in Table 2. The thermal behaviors of NICs were studied by TG analysis.

Table 2. Surface and pore characteristics of the NICs adsorbents.

Parameter	Unit	PB Clay	BT Clay	RM Clay
Surface Area	m^2/g	115.99	38.306	16.796
Pore Volume	cm^3/g	0.1527	0.0711	0.0656
Pore Size	nm	9.6055	19.168	25.834

It is clear from Figure 7 that a continuous weight loss was observed for all the clay minerals in the test temperature range. A two-step weight loss of 9.8%, 8.7%, and 7.5%

was observed for PB, BT, and RM adsorbents, respectively. The first weight loss due to the dehydration of adsorbed water occurred over the 30 °C to 160 °C temperature range, while the second weight loss over the 200 °C to 650 °C temperature range occurred due to the loss of hydrated cations on the exchangeable sites and interlayer water dehydration of the NICs adsorbents.
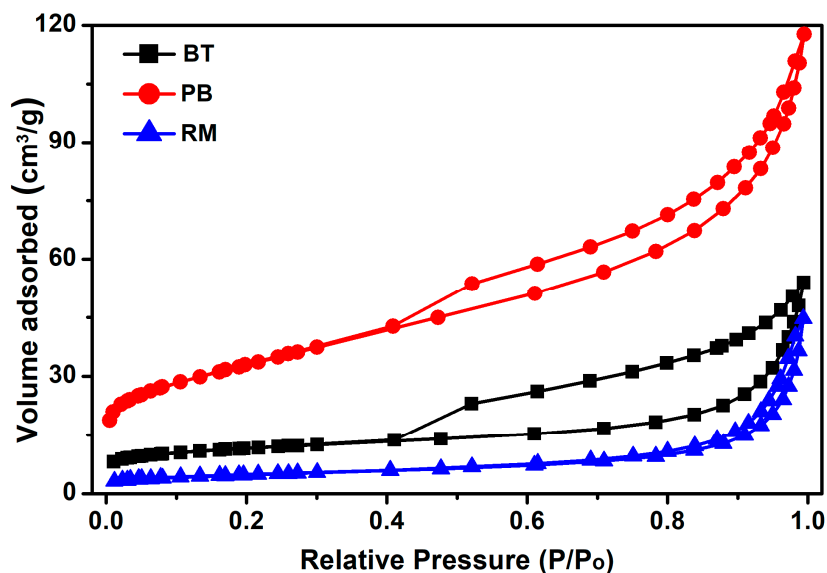

Figure 6. Brunauer–Emmett–Teller (BET) N_2 adsorption-desorption isotherms plot of the NICs sorbent.
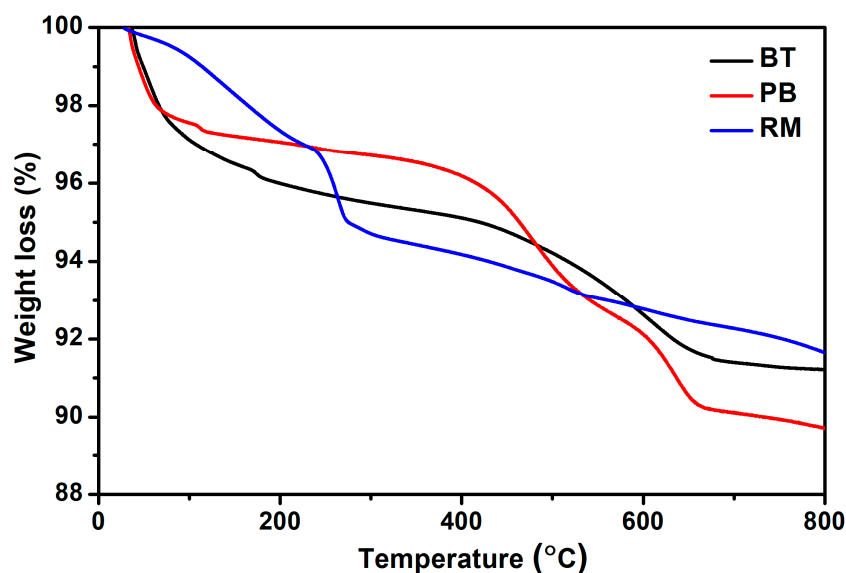
Figure 7. Thermogravimetric analysis (TGA) of BT, PB, and RM adsorbent.

3.2. Adsorption Studies of MG Dye

The adsorption behaviors of the NICs were examined to assess their potential applications in the decontamination of wastewater containing organic dyes. The influence of adsorption time, aqueous phase pH, MG concentration, and the amount of NICs on the decolorization capabilities of NICs were evaluated under batch conditions.

The adsorption uptake of MG by the NICs under varied periods of adsorption contact time (10 to 120 min) is shown in Figure 8. During the experiments, the adsorption capacities increased with the increase in the adsorption contact time. Initially, the rate of dye uptake was high, and afterward, a gradual decrease was observed until the equilib-

rium was attained [53]. This trend of variation in the MG uptake rates was related to the availability of adsorbent surface active sites. In the beginning, the faster adsorption rates were attributed to the abundant surface-active sites that saturated over time and opposed further adsorption [54,55].
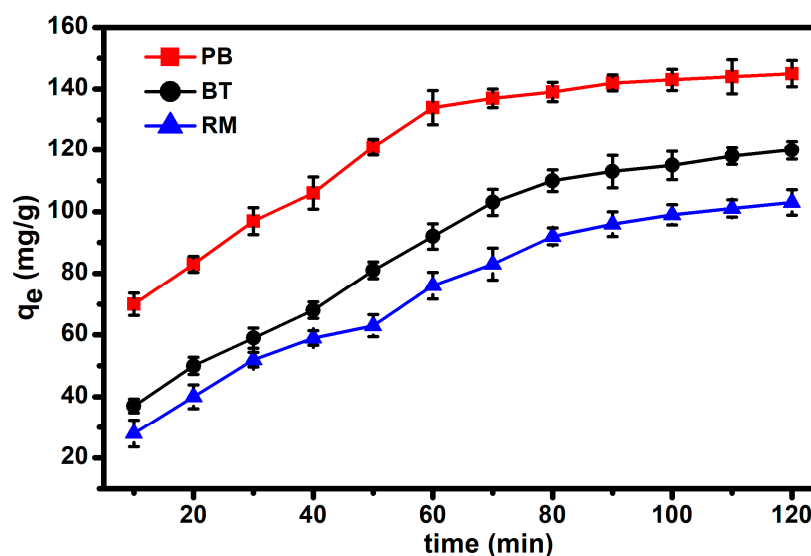

Figure 8. Effect of contact time on malachite green (MG) adsorption.

The initial solution pH is a foremost significant controlling parameter in the process of dye adsorption, as it can directly influence the adsorbent surface charges, the solute's dissociation, and as the adsorption mechanism [56]. It is also associated with the structural changes and color intensities of dye molecules and is directly related to the competitive adsorption process between the MG molecules and hydrogen ions [57]. The influence of initial pH on the adsorption characteristics of MG by NICs adsorbents was examined in the pH range of 3–11. According to the results (Figure 9), the adsorption capacities of NICs adsorbents increased from 45.6 to 130.8 mg/g for RM, 62.4 to 142.8 mg/g for BT, and 82.8 to 170.6 mg/g for PB, with the increase of pH of MG solution from 3 to 11, respectively. In an alkaline environment, the surface functional groups (Si-OH and Al-OH) of the NICs were deprotonated by –OH, due to which the surface became negatively charged; as a result, the electrostatic interaction between anionic NICs surfaced and cationic MG molecules increased [1], whereas at low solution pH, the H+ ions concentration was very high, thus competing intensely with the cationic dye to occupy the adsorption site, therefore causing a reduction in the adsorption of MG dye [58].

It is essential to analyze the effect of the adsorbent amount, to optimize and select the best-required dose of an adsorbent for scaling-up and designing large-scale equipment [59]. The influence of adsorbent dosage on dye adsorption is presented in Figure 10. The obtained results show that increasing the NICs dose from 0.1 to 0.5 g resulted in decreases in the adsorption capacities from 76 to 23.4 mg/g for RM, 92 to 27.4 mg/g for BT, and 134 to 29.6 mg/g for PB. The resulted decrease in adsorption capacities is due to the increasing NICs dose (0.1 to 0.5 g), while the number of MG molecules remained fixed ($Ce = 100$ mg/L). Hence, at a higher NICs dose, some of the surface-active sites of the NICs remained empty [60].

To determine the influence of the initial MG concentration on the adsorption capacities, the experiments were performed by changing the concentration in the range of 100–350 mg/L, keeping other conditions constant. The results are shown in Figure 11. It was determined that the adsorption capacities of MG onto NICs adsorbents increased from 92 to 223 mg/g for PB, 69 to 149 mg/g for BT, and 57 to 125 mg/g for RM as the initial concentration increased from 100 to 350 mg/L. Moreover, at higher concentrations, the adsorption uptake rate was also higher due to the higher concentration gradient [61].
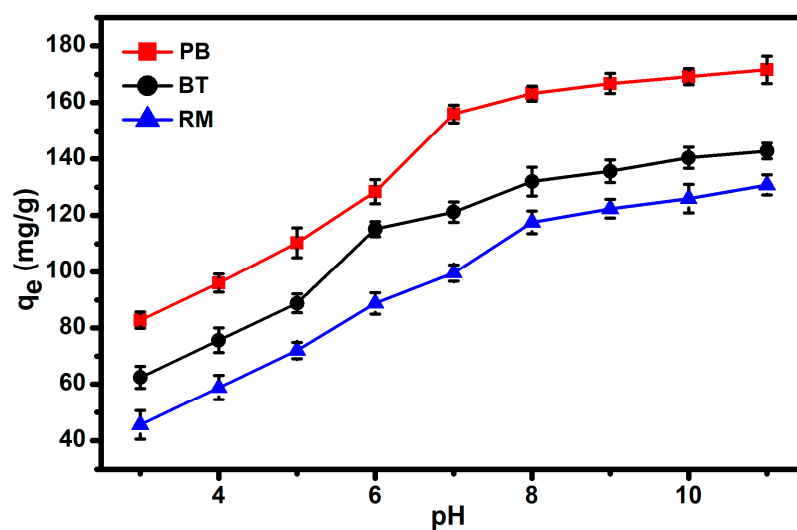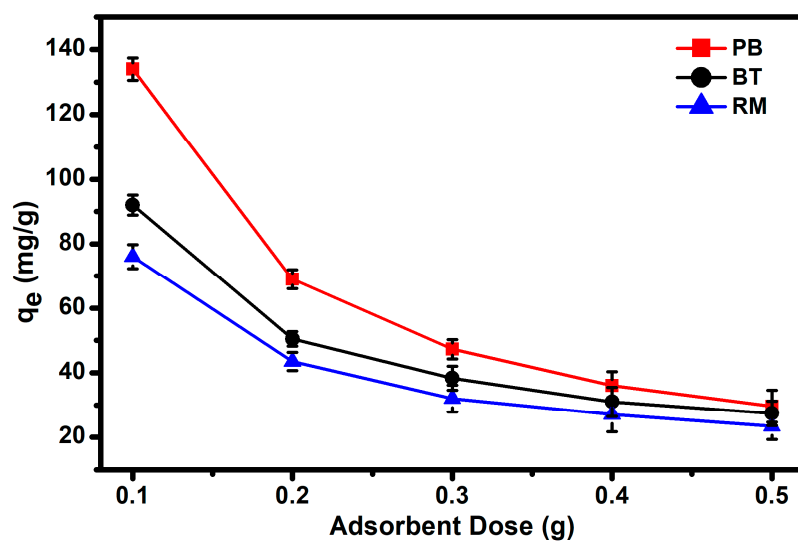
Figure 9. Effect of pH on MG adsorption.

Figure 10. Effect of adsorbent dose on MG adsorption.
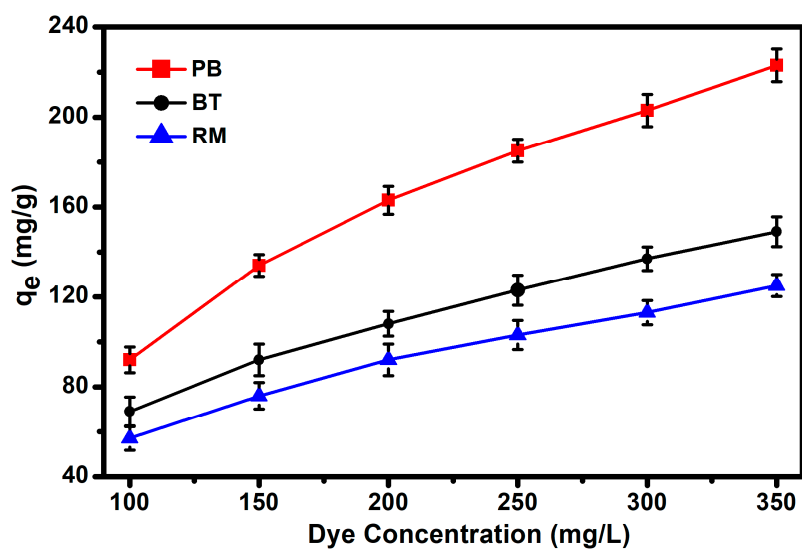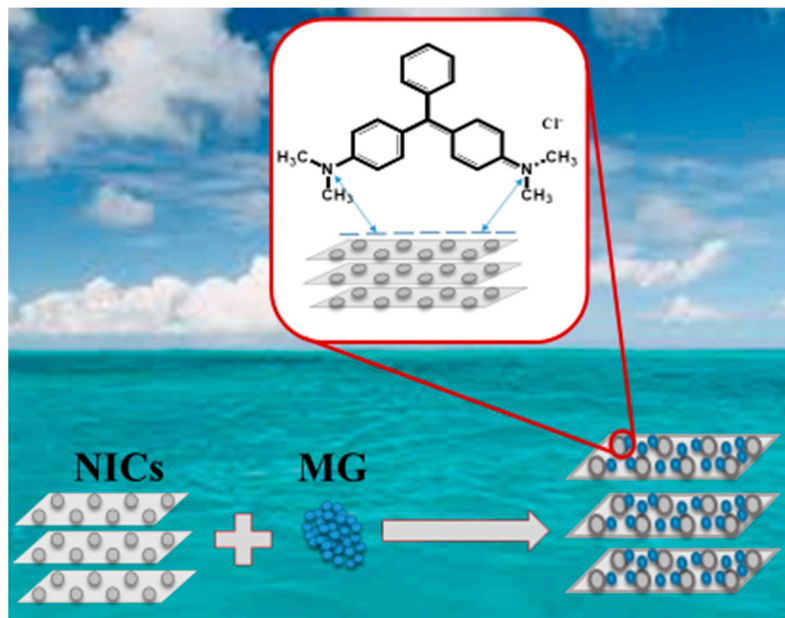

Figure 11. Effect of initial dye concentration on MG adsorption.

By taking into account the above experimental data and analysis, a mechanism for the electrostatic interactions between the MG and NICs was proposed, as illustrated in Figure 12.

Figure 12. The adsorption mechanism of MG onto NICs.

3.3. Adsorption Kinetics

Adsorption kinetics analysis was carried out to describe the rate of adsorbate uptake and evaluate the adsorption mechanism. The adsorption process occurs mainly in three steps; (i) the external mass transfer of the adsorbate molecules from the bulk solution to the external adsorbent surface, (ii) transfer of adsorbed molecules to the adsorption sites, (iii) and finally, retention via sorption itself [62]. Therefore, the experimental data were inspected by the two different kinetic models, namely the pseudo-first-order and pseudo-second-order kinetics model.

The pseudo-first-order kinetic model can be represented as follows [55]:

$$\log(q_e - q_t) = \log q_e - \frac{k_1}{2.303}t \tag{2}$$

where k_1 (min^{-1}) is the pseudo-first-order rate constant, q_e and q_t are the adsorption capacities (mg/g) at equilibrium and at any time t (min), respectively.

The empirical equation for the pseudo-second-order kinetic model is [63]:

$$\frac{d_{q_t}}{d_t} = k_2(q_e - q_t)^2 \tag{3}$$

Integrating and rearranging Equation (3), we received

$$\frac{t}{q_t} = \frac{1}{k_2 q_e{}^2} + \frac{1}{q_e}t \tag{4}$$

where k_2 (g/mg. min) is the pseudo-second-order model rate constant.

The linear fitting kinetic results are presented in Figure 13a,b and the calculated kinetic parameters are given in Table 3. When the regression coefficients (R^2) values of the used models were compared, it was found that they have almost the same values for R^2. However, the experimental (q_{exp}) values of the pseudo-first-order model were found close

to the calculated (q_e) as compared to the pseudo-second-order model, which confirms that the adsorption of MG was followed by the pseudo-first-order model.
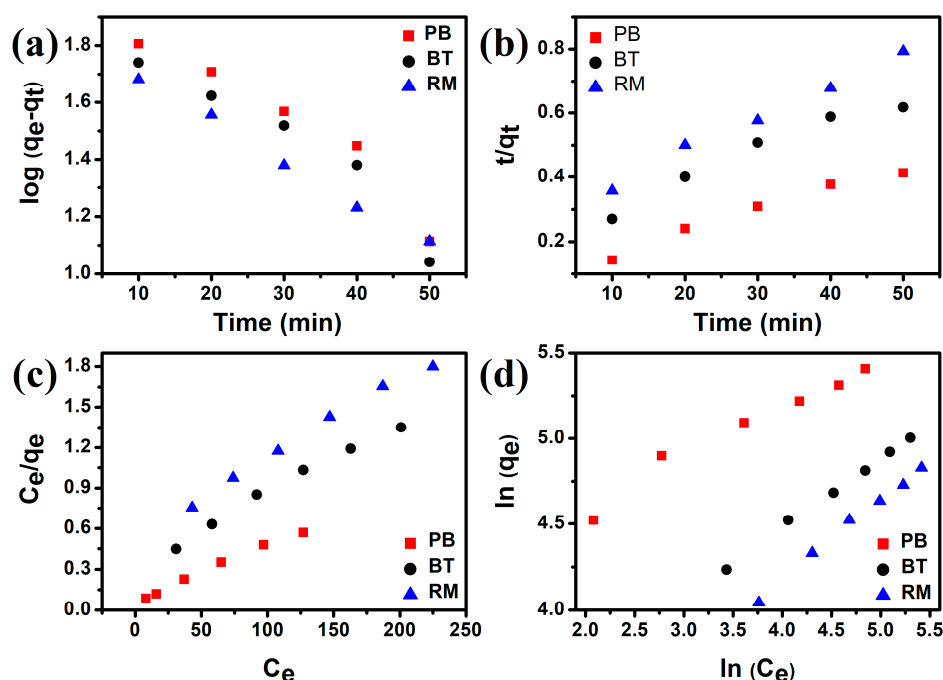
Figure 13. (**a**) Pseudo-first-order and (**b**) pseudo-second-order kinetic models; (**c**) Langmuir isotherm and (**d**) Freundlich isotherm model for MG adsorption onto NICs adsrobents.

Table 3. Kinetic data predicted by pseudo-first-order and pseudo-second-order kinetic models for the adsorption of MG onto NICs adsorbents.

Adsorbent		Pseudo-First Order				Pseudo-Second Order		
	Dye	$q_{(exp)}$ (mg/g)	$q_{e\ (calc)}$ (mg/g)	K_1 (min^{-1})	R^2	$q_{e\ (calc)}$ (mg/g)	K_2 (mg/g)	R^2
PB clay	MG	134	105.22	0.01645	0.935	147.06	0.007	0.975
BT clay	MG	92	89.74	0.01641	0.928	113.63	0.009	0.953
RM clay	MG	76	67.70	0.01460	0.996	95.24	0.010	0.992

3.4. Adsorption Isotherm

The adsorption isotherm studies provide helpful information to understand the nature of the interaction between the adsorbed matter and adsorbent, and to evaluate the efficiency of the adsorbent material used for adsorption. The experimental data were evaluated by two commonly used adsorption isotherm models, namely the Freundlich and Langmuir models. According to the Langmuir model, adsorption of analyte takes place on the homogenous sites the adsorbent with the monolayer formation [63], and can be expressed as:

$$\frac{C_e}{q_e} = \frac{1}{K_L q_m} + \frac{C_e}{q_m} \tag{5}$$

where K_L (L/mg) represents the adsorption equilibrium constant for the Langmuir model and is related to the adsorption energy, q_e and q_m are the equilibrium adsorption amount of adsorbate and monolayer adsorption capacity of adsorbents in the experiments (mg/g), respectively, and Ce (mg/L) is equilibrium adsorbate concentration.

The Freundlich isotherm, applied to non-ideal and reversible adsorption, is valid for multilayer adsorption of analyte and can be expressed as:

$$l_n q_e = l_n K_F + \frac{1}{n_F} l_n C_e \qquad (6)$$

where K_F (mg/g) represents the Freundlich constant and $1/n$ is the heterogeneity factor.

All of the correlation coefficients and constants obtained from the used adsorption isotherm models were summarized in Table 4. The results show that both of the isotherms have very high R^2; however, experimental maximum adsorption capacities are close to the q_m calculated from the Langmuir isotherm model. The results show that adsorption of MG onto the surface of NICs adsorbents occurs via monolayer formation.

Table 4. Langmuir and Freundlich parameters for the adsorption of MG onto NICs adsorbents.

Adsorbent	Dye	Langmuir						Freundlich	
		$q_{(exp)}$ (mg/g)	q_m (mg/g)	K_L (L/mg)	R^2	R_L	n_F	K_F (mg/g)	R^2
PB clay	MG	223	243.90	0.064	0.994	0.135	3.373	53.83	0.968
BT clay	MG	149	188.68	0.016	0.990	0.382	2.462	17.30	0.998
RM clay	MG	125	172.41	0.011	0.993	0.481	2.153	10.15	0.995

A direct comparison of the adsorption capacities obtained in this study and earlier reported in the literature is difficult due to the varying experimental conditions employed in those studies. However, from Table 5, it can be concluded that the NICs used in this study provide better results for MG adsorption than the others reported in the literature.

Table 5. Comparison of the maximum adsorption capacities of some adsorbents used for MG dye.

Adsorbent	Isotherm	q_m (mg/g)	References
Kaolin	Langmuir	52	[64]
Clayey soil	Langmuir	78.57	[65]
Diatomite	Langmuir	23.64	[66]
Rattan sawdust	Langmuir	62.71	[67]
Wood apple shell	Langmuir	34.56	[68]
Walnut shell	Langmuir	90.8	[69]
Conch shell powder	Langmuir	92.25	[70]
Sea shell powder	Langmuir	42.33	[21]
PB clay	Langmuir	223	This study
BT clay	Langmuir	149	This study
RM clay	Langmuir	125	This study

4. Conclusions

In the current study, three different mesoporous natural clays were used as an environment-friendly, efficient, easily available, and low-cost material for the adsorption of cationic MG dye from an aqueous environment. The chemical composition, mineralogical composition, and texture of NICs were determined by using XRF, XRD, FESEM, FTIR, BET, and TGA analysis. It was observed that PB clay has a quite rough surface with blunt edges and higher surface area as compared to the BT clay and RM clay. The experimental results indicated that adsorption removal of MG was highly dependent on the adsorption contact time, aqueous pH, NICs dose, and MG concentration. The adsorption capacities of MG onto NICs increased with the increase in the adsorption contact time, pH, and MG concentration, while it decreased with the increase in NICs dose. Furthermore, the kinetics data fitted the pseudo-first-order model well. The isotherm data illustrated the suitability of employing the Langmuir isotherm model. The adsorption capacity of PB clay (223 mg/g) was found higher than the BT clay (149 mg/g) and RM clay (125 mg/g). The adsorption of MG dye was more correlated to the BET surface area and available binding sites of the

adsorbent material. Conclusively, naturally occurring mesoporous clays can be efficiently applied for the removal of cationic dyes from contaminated environs.

References

1. Gamoudi, S.; Srasra, E. Adsorption of organic dyes by HDPy+-modified clay: Effect of molecular structure on the adsorption. *J. Mol. Struct.* **2019**, *1193*, 522–531. [CrossRef]
2. Garg, D.; Kumar, S.; Sharma, K.; Majumder, C. Application of waste peanut shells to form activated carbon and its utilization for the removal of Acid Yellow 36 from wastewater. *Groundw. Sustain. Dev.* **2019**, *8*, 512–519. [CrossRef]
3. Rashid, A.; Khan, S.; Ayub, M.; Sardar, T.; Jehan, S.; Zahir, S.; Khan, M.S.; Muhammad, J.; Khan, R.; Ali, A. Mapping human health risk from exposure to potential toxic metal contamination in groundwater of Lower Dir, Pakistan: Application of multivariate and geographical information system. *Chemosphere* **2019**, *225*, 785–795. [CrossRef]
4. Amarasooriya, A.; Kawakami, T. Removal of fluoride, hardness and alkalinity from groundwater by electrolysis. *Groundw. Sustain. Dev.* **2019**, *9*, 100231. [CrossRef]
5. Adebayo, T.B.; Abegunrin, T.P.; Awe, G.O.; Are, K.S.; Guo, H.; Onofua, O.E.; Adegbola, G.A.; Ojediran, J.O. Geospatial mapping and suitability classification of groundwater quality for agriculture and domestic uses in a Precambrian basement complex. *Groundw. Sustain. Dev.* **2021**, *12*, 100497. [CrossRef]
6. Ahmed, M.; Mashkoor, F.; Nasar, A. Development, characterization, and utilization of magnetized orange peel waste as a novel adsorbent for the confiscation of crystal violet dye from aqueous solution. *Groundw. Sustain. Dev.* **2020**, *10*, 100322. [CrossRef]
7. Priya, K.; Aswin, K.; Indu, M.; Adarsh, S. Assessment of hydrogeochemical processes in the aquifers of Coimbatore city, India with special reference to nickel contamination. *Groundw. Sustain. Dev.* **2020**, *11*, 100393. [CrossRef]
8. Bolisetty, S.; Peydayesh, M.; Mezzenga, R. Sustainable technologies for water purification from heavy metals: Review and analysis. *Chem. Soc. Rev.* **2019**, *48*, 463–487. [CrossRef] [PubMed]
9. Pillai, P.; Dharaskar, S.; Shah, M.; Sultania, R. Determination of fluoride removal using silica nano adsorbent modified by rice husk from water. *Groundw. Sustain. Dev.* **2020**, *11*, 100423. [CrossRef]
10. Hou, M.-F.; Ma, C.-X.; Zhang, W.-D.; Tang, X.-Y.; Fan, Y.-N.; Wan, H.-F. Removal of rhodamine B using iron-pillared bentonite. *J. Hazard. Mater.* **2011**, *186*, 1118–1123. [CrossRef]
11. Chu, H.; Liu, X.; Liu, B.; Zhu, G.; Lei, W.; Du, H.; Liu, J.; Li, J.; Li, C.; Sun, C. Hexagonal 2H-MoSe 2 broad spectrum active photocatalyst for Cr (VI) reduction. *Sci. Rep.* **2016**, *6*, 1–10. [CrossRef] [PubMed]
12. Saeed, M.; Munir, M.; Nafees, M.; Shah, S.S.A.; Ullah, H.; Waseem, A. Synthesis, characterization and applications of silylation based grafted bentonites for the removal of Sudan dyes: Isothermal, kinetic and thermodynamic studies. *Microporous Mesoporous Mater.* **2020**, *291*, 109697. [CrossRef]
13. Sarma, G.K.; Gupta, S.S.; Bhattacharyya, K.G. *RETRACTED: Adsorption of Crystal Violet on Raw and Acid-Treated Montmorillonite, K10, in Aqueous Suspension*; Elsevier: Amsterdam, The Netherlands, 2016.
14. Hou, H.; Zhou, R.; Wu, P.; Wu, L. Removal of Congo red dye from aqueous solution with hydroxyapatite/chitosan composite. *Chem. Eng. J.* **2012**, *211*, 336–342. [CrossRef]
15. Tsai, W.; Chang, C.; Lin, M.; Chien, S.; Sun, H.; Hsieh, M. Adsorption of acid dye onto activated carbons prepared from agricultural waste bagasse by ZnCl$_2$ activation. *Chemosphere* **2001**, *45*, 51–58. [CrossRef]
16. Raghu, M.; Kumar, K.Y.; Prashanth, M.; Prasanna, B.; Vinuth, R.; Kumar, C.P. Adsorption and antimicrobial studies of chemically bonded magnetic graphene oxide-Fe$_3$O$_4$ nanocomposite for water purification. *J. Water Process Eng.* **2017**, *17*, 22–31. [CrossRef]
17. Crini, G.; Peindy, H.N.; Gimbert, F.; Robert, C. Removal of CI Basic Green 4 (Malachite Green) from aqueous solutions by adsorption using cyclodextrin-based adsorbent: Kinetic and equilibrium studies. *Sep. Purif. Technol.* **2007**, *53*, 97–110. [CrossRef]
18. Tsai, W.-T.; Chen, H.-R. Removal of malachite green from aqueous solution using low-cost chlorella-based biomass. *J. Hazard. Mater.* **2010**, *175*, 844–849. [CrossRef] [PubMed]

19. Saha, P.; Chowdhury, S.; Gupta, S.; Kumar, I.; Kumar, R. Assessment on the removal of malachite green using tamarind fruit shell as biosorbent. *Clean Soil Air Water* **2010**, *38*, 437–445. [CrossRef]

20. Srivastava, S.; Sinha, R.; Roy, D. Toxicological effects of malachite green. *Aquat. Toxicol.* **2004**, *66*, 319–329. [CrossRef] [PubMed]

21. Chowdhury, S.; Saha, P. Sea shell powder as a new adsorbent to remove Basic Green 4 (Malachite Green) from aqueous solutions: Equilibrium, kinetic and thermodynamic studies. *Chem. Eng. J.* **2010**, *164*, 168–177. [CrossRef]

22. Nethaji, S.; Sivasamy, A.; Thennarasu, G.; Saravanan, S. Adsorption of Malachite Green dye onto activated carbon derived from Borassus aethiopum flower biomass. *J. Hazard. Mater.* **2010**, *181*, 271–280. [CrossRef] [PubMed]

23. Duan, Y.; Song, Y.; Zhou, L. Facile synthesis of polyamidoamine dendrimer gel with multiple amine groups as a super adsorbent for highly efficient and selective removal of anionic dyes. *J. Colloid Interface Sci.* **2019**, *546*, 351–360. [CrossRef]

24. Kheirabadi, M.; Samadi, M.; Asadian, E.; Zhou, Y.; Dong, C.; Zhang, J.; Moshfegh, A.Z. Well-designed Ag/ZnO/3D graphene structure for dye removal: Adsorption, photocatalysis and physical separation capabilities. *J. Colloid Interface Sci.* **2019**, *537*, 66–78. [CrossRef]

25. Yuan, Y.-J.; Chen, D.; Yu, Z.-T.; Zou, Z.-G. Cadmium sulfide-based nanomaterials for photocatalytic hydrogen production. *J. Mater. Chem. A* **2018**, *6*, 11606–11630. [CrossRef]

26. Fu, J.; Yu, J.; Jiang, C.; Cheng, B. g-C3N4-Based heterostructured photocatalysts. *Adv. Energy Mater.* **2018**, *8*, 1701503. [CrossRef]

27. SMoghaddam, S.; Moghaddam, M.A.; Arami, M. Coagulation/flocculation process for dye removal using sludge from water treatment plant: Optimization through response surface methodology. *J. Hazard. Mater.* **2010**, *175*, 651–657. [CrossRef] [PubMed]

28. Chen, X.; Zhao, Y.; Moutinho, J.; Shao, J.; Zydney, A.L.; He, Y. Recovery of small dye molecules from aqueous solutions using charged ultrafiltration membranes. *J. Hazard. Mater.* **2015**, *284*, 58–64. [CrossRef]

29. Ikhlaq, A.; Brown, D.R.; Kasprzyk-Hordern, B. Catalytic ozonation for the removal of organic contaminants in water on alumina. *Appl. Catal. B Environ.* **2015**, *165*, 408–418. [CrossRef]

30. Jayanthi, S.; Eswar, N.K.; Singh, S.A.; Chatterjee, K.; Madras, G.; Sood, A. Macroporous three-dimensional graphene oxide foams for dye adsorption and antibacterial applications. *RSC Adv.* **2016**, *6*, 1231–1242. [CrossRef]

31. Bentahar, S.; Dbik, A.; el Khomri, M.; el Messaoudi, N.; Lacherai, A. Adsorption of methylene blue, crystal violet and congo red from binary and ternary systems with natural clay: Kinetic, isotherm, and thermodynamic. *J. Environ. Chem. Eng.* **2017**, *5*, 5921–5932. [CrossRef]

32. Basaleh, A.A.; Al-Malack, M.H.; Saleh, T.A. Methylene Blue removal using polyamide-vermiculite nanocomposites: Kinetics, equilibrium and thermodynamic study. *J. Environ. Chem. Eng.* **2019**, *7*, 103107. [CrossRef]

33. Alkan, M.; Doğan, M.; Turhan, Y.; Demirbaş, Ö.; Turan, P. Adsorption kinetics and mechanism of maxilon blue 5G dye on sepiolite from aqueous solutions. *Chem. Eng. J.* **2008**, *139*, 213–223. [CrossRef]

34. Chakraborty, S.; Chowdhury, S.; Saha, P.D. Adsorption of crystal violet from aqueous solution onto sugarcane bagasse: Central composite design for optimization of process variables. *J. Water Reuse Desalin.* **2012**, *2*, 55–65. [CrossRef]

35. Mittal, A.; Mittal, J.; Malviya, A.; Kaur, D.; Gupta, V. Adsorption of hazardous dye crystal violet from wastewater by waste materials. *J. Colloid Interface Sci.* **2010**, *343*, 463–473. [CrossRef] [PubMed]

36. Chen, H.; Zhao, J.; Zhong, A.; Jin, Y. Removal capacity and adsorption mechanism of heat-treated palygorskite clay for methylene blue. *Chem. Eng. J.* **2011**, *174*, 143–150. [CrossRef]

37. De Queiroga, L.N.F.; Franca, D.B.; Rodrigues, F.; Santos, I.M.; Fonseca, M.G.; Jaber, M. Functionalized bentonites for dye adsorption: Depollution and production of new pigments. *J. Environ. Chem. Eng.* **2019**, *7*, 103333. [CrossRef]

38. Vimonses, V.; Lei, S.; Jin, B.; Chow, C.W.; Saint, C. Kinetic study and equilibrium isotherm analysis of Congo Red adsorption by clay materials. *Chem. Eng. J.* **2009**, *148*, 354–364. [CrossRef]

39. Olusegun, S.J.; Lima, L.F.d.; Mohallem, N.D.S. Enhancement of adsorption capacity of clay through spray drying and surface modification process for wastewater treatment. *Chem. Eng. J.* **2018**, *334*, 1719–1728. [CrossRef]

40. Munir, M.; Nazar, M.F.; Zafar, M.N.; Zubair, M.; Ashfaq, M.; Hosseini-Bandegharaei, A.; Khan, S.U.-D.; Ahmad, A. Effective Adsorptive Removal of Methylene Blue from Water by Didodecyldimethylammonium Bromide-Modified Brown Clay. *ACS Omega* **2020**, *5*, 16711–16721. [CrossRef]

41. Brito, D.F.; Filho, E.C.d.; Fonseca, M.G.; Jaber, M. Organophilic bentonites obtained by microwave heating as adsorbents for anionic dyes. *J. Environ. Chem. Eng.* **2018**, *6*, 7080–7090. [CrossRef]

42. Javed, S.H.; Zahir, A.; Khan, A.; Afzal, S.; Mansha, M. Adsorption of Mordant Red 73 dye on acid activated bentonite: Kinetics and thermodynamic study. *J. Mol. Liq.* **2018**, *254*, 398–405. [CrossRef]

43. Elmoubarki, R.; Mahjoubi, F.; Tounsadi, H.; Moustadraf, J.; Abdennouri, M.; Zouhri, A.; el Albani, A.; Barka, N. Adsorption of textile dyes on raw and decanted Moroccan clays: Kinetics, equilibrium and thermodynamics. *Water Resour. Ind.* **2015**, *9*, 16–29. [CrossRef]

44. Chaari, I.; Fakhfakh, E.; Medhioub, M.; Jamoussi, F. Comparative study on adsorption of cationic and anionic dyes by smectite rich natural clays. *J. Mol. Struct.* **2019**, *1179*, 672–677. [CrossRef]

45. Agatzini-Leonardou, S.; Oustadakis, P.; Tsakiridis, P.; Markopoulos, C. Titanium leaching from red mud by diluted sulfuric acid at atmospheric pressure. *J. Hazard. Mater.* **2008**, *157*, 579–586. [CrossRef] [PubMed]

46. Makhoukhi, B.; Djab, M.; Didi, M.A. Adsorption of Telon dyes onto bis-imidazolium modified bentonite in aqueous solutions. *J. Environ. Chem. Eng.* **2015**, *3*, 1384–1392. [CrossRef]

47. Madejová, J. FTIR techniques in clay mineral studies. *Vib. Spectrosc.* **2003**, *31*, 1–10. [CrossRef]

48. Toor, M.; Jin, B.; Dai, S.; Vimonses, V. Activating natural bentonite as a cost-effective adsorbent for removal of Congo-red in wastewater. *J. Ind. Eng. Chem.* **2015**, *21*, 653–661. [CrossRef]

49. Jawad, A.H.; Abdulhameed, A.S. Mesoporous Iraqi red kaolin clay as an efficient adsorbent for methylene blue dye: Adsorption kinetic, isotherm and mechanism study. *Surf. Interfaces* **2020**, *18*, 100422. [CrossRef]

50. Hassanien, M.M.; Abou-El-Sherbini, K.S.; Al-Muaikel, N.S. Immobilization of methylene blue onto bentonite and its application in the extraction of mercury (II). *J. Hazard. Mater.* **2010**, *178*, 94–100. [CrossRef]

51. Ahmadi, A.; Foroutan, R.; Esmaeili, H.; Tamjidi, S. The role of bentonite clay and bentonite clay@ $MnFe_2O_4$ composite and their physico-chemical properties on the removal of Cr (III) and Cr (VI) from aqueous media. *Environ. Sci. Pollut. Res.* **2020**, *27*, 1–14. [CrossRef]

52. el Ouardi, M.; Laabd, M.; Oualid, H.A.; Brahmi, Y.; Abaamrane, A.; Elouahli, A.; Addi, A.A.; Laknifli, A. Efficient removal of p-nitrophenol from water using montmorillonite clay: Insights into the adsorption mechanism, process optimization, and regeneration. *Environ. Sci. Pollut. Res.* **2019**, *26*, 19615–19631. [CrossRef] [PubMed]

53. Marrakchi, F.; Khanday, W.; Asif, M.; Hameed, B. Cross-linked chitosan/sepiolite composite for the adsorption of methylene blue and reactive orange 16. *Int. J. Biol. Macromol.* **2016**, *93*, 1231–1239. [CrossRef]

54. Bentahar, S.; Dbik, A.; el Khomri, M.; el Messaoudi, N.; Lacherai, A. Removal of a cationic dye from aqueous solution by natural clay. *Groundw. Sustain. Dev.* **2018**, *6*, 255–262. [CrossRef]

55. Ullah, H.; Nafees, M.; Iqbal, F.; Awan, S.; Shah, A.; Waseem, A. Adsorption Kinetics of Malachite green and Methylene blue from aqueous solutions using surfactant-modified Organoclays. *Acta Chim. Slov.* **2017**, *64*, 449–460. [CrossRef] [PubMed]

56. Doğan, M.; Özdemir, Y.; Alkan, M. Adsorption kinetics and mechanism of cationic methyl violet and methylene blue dyes onto sepiolite. *Dye. Pigment.* **2007**, *75*, 701–713. [CrossRef]

57. Munagapati, V.S.; Yarramuthi, V.; Nadavala, S.K.; Alla, S.R.; Abburi, K. Biosorption of Cu (II), Cd (II) and Pb (II) by *Acacia leucocephala* bark powder: Kinetics, equilibrium and thermodynamics. *Chem. Eng. J.* **2010**, *157*, 357–365. [CrossRef]

58. Fil, B.A. Isotherm, kinetic, and thermodynamic studies on the adsorption behavior of malachite green dye onto montmorillonite clay. *Part. Sci. Technol.* **2016**, *34*, 118–126. [CrossRef]

59. Ghanizadeh, G.; Asgari, G. Adsorption kinetics and isotherm of methylene blue and its removal from aqueous solution using bone charcoal. *React. Kinet. Mech. Catal.* **2011**, *102*, 127–142. [CrossRef]

60. Rehman, M.S.U.; Munir, M.; Ashfaq, M.; Rashid, N.; Nazar, M.F.; Danish, M.; Han, J.-I. Adsorption of Brilliant Green dye from aqueous solution onto red clay. *Chem. Eng. J.* **2013**, *228*, 54–62. [CrossRef]

61. Karim, A.B.; Mounir, B.; Hachkar, M.; Bakasse, M.; Yaacoubi, A. Removal of Basic Red 46 dye from aqueous solution by adsorption onto Moroccan clay. *J. Hazard. Mater.* **2009**, *168*, 304–309. [CrossRef] [PubMed]

62. Bhatti, H.N.; Zaman, Q.; Kausar, A.; Noreen, S.; Iqbal, M. Efficient remediation of Zr (IV) using citrus peel waste biomass: Kinetic, equilibrium and thermodynamic studies. *Ecol. Eng.* **2016**, *95*, 216–228. [CrossRef]

63. Ullah, R.; Iftikhar, F.J.; Ajmal, M.; Shah, A.; Akhter, M.S.; Ullah, H.; Waseem, A. Modified clays as an efficient adsorbent for brilliant green, ethyl violet and allura red dyes: Kinetic and thermodynamic Studies. *Pol. J. Environ. Stud.* **2020**, *29*, 3831–3839. [CrossRef]

64. Tehrani-Bagha, A.; Nikkar, H.; Mahmoodi, N.; Markazi, M.; Menger, F. The sorption of cationic dyes onto kaolin: Kinetic, isotherm and thermodynamic studies. *Desalination* **2011**, *266*, 274–280. [CrossRef]

65. Saha, P.; Chowdhury, S.; Gupta, S.; Kumar, I. Insight into adsorption equilibrium, kinetics and thermodynamics of Malachite Green onto clayey soil of Indian origin. *Chem. Eng. J.* **2010**, *165*, 874–882. [CrossRef]

66. Tian, L.; Zhang, J.; Shi, H.; Li, N.; Ping, Q. Adsorption of malachite green by diatomite: Equilibrium isotherms and kinetic studies. *J. Dispers. Sci. Technol.* **2016**, *37*, 1059–1066. [CrossRef]

67. Hameed, B.; El-Khaiary, M. Malachite green adsorption by rattan sawdust: Isotherm, kinetic and mechanism modeling. *J. Hazard. Mater.* **2008**, *159*, 574–579. [CrossRef]

68. Sartape, A.S.; Mandhare, A.M.; Jadhav, V.V.; Raut, P.D.; Anuse, M.A.; Kolekar, S.S. Removal of malachite green dye from aqueous solution with adsorption technique using *Limonia acidissima* (wood apple) shell as low cost adsorbent. *Arab. J. Chem.* **2017**, *10*, S3229–S3238. [CrossRef]

69. Dahri, M.K.; Kooh, M.R.R.; Lim, L.B. Water remediation using low cost adsorbent walnut shell for removal of malachite green: Equilibrium, kinetics, thermodynamic and regeneration studies. *J. Environ. Chem. Eng.* **2014**, *2*, 1434–1444. [CrossRef]

70. Chowdhury, S.; Das, P. Mechanistic, kinetic, and thermodynamic evaluation of adsorption of hazardous malachite green onto conch shell powder. *Sep. Sci. Technol.* **2011**, *46*, 1966–1976. [CrossRef]